Scalable Computing: Practice and Experience, ISSN 1895-1767, http://www.scpe.org
© 2025 SCPE. Volume 26, Issues 1, pp. 1–15, DOI 10.12694/scpe.v26i1.3432

ANALYZING HISTOPATHOLOGICAL IMAGES FOR CANCER PREDICTION USING HUMAN CENTRIC LEARNING APPROACHES

N HARI BABU *AND VAMSIDHAR ENIREDDY†

Abstract. Examining Histopathological images are a substantial approach for earlier cancer prediction in clinical analysis. However, the examination encounters some inefficiency; therefore, the cancer prediction process is depicted as a significant issue in medical imaging analysis. To simulate the prediction accuracy and to diminish the expert's decision-making complexity, this work proposes a novel feature extraction and selection of histopathological images by integrating deep learning and machine learning approaches. Initially, the provided input samples are pre-processed via dimensionality reduction, RGB colour analysis, and image transformation. Then, the features are extracted with the pre-trained network model like AlexNet, GoogleNet, Inception V3, and ResNet 50. Next, feature selection is done with Recursive Feature Elimination (RFE) to enhance and boost the system performance and eliminate over-fitting or under-fitting issues. The proposed model is evaluated with the key evaluation parameters like accuracy, precision and recall. At last, a non-linear Support Vector Machine ($nl-SVM$) is trained to fuse the related features and to enhance the performance outcomes. Here, an online available dataset for histology image-based cancer analysis is adopted. The observation proves that the anticipated model gives promising outcomes and better results than various prevailing approaches.

Key words: Histopathological images, prediction, deep learning, machine learning, feature representation

1. Introduction. Recently, the branch of digitized tissue histopathology has used computer-aided diagnosis and computerized image processing for automatic disease grading and microscopic evaluation [1]. Several strategies have been implemented to address this challenging and vital use case, such as evaluating object-level and spatially connected data, applying content-based image retrieval (CBIR) and learning-based classifiers [2]. Studying cell-level data, which includes individual cells (such as appearance) and tissue architecture (such as topology and arrangement of all cells), is essential to obtain correct histopathological image analysis for an acceptable diagnosis [3]. These components include local and global data, and they work together to improve the accuracy of histopathology image diagnosis. Given both local and holistic elements serve different descriptive purposes, the challenge of successfully combining their advantages to identify histopathological images satisfactorily naturally arises [4]. However, these components' characteristics, computing methods, and representations could be very different, which presents difficulties for the fusion process. Local features are depicted as bag-of-words (BoW) with a high-dimensional structure and subsequently compressed into binary codes. On the other hand, architectural features are characterized by a low-dimensional statistical vector [5].

In the field of cancer differentiation, fusion techniques can be utilized either at the level of features or ranks [6]. In our particular domain, this includes integrating the ordered results from content-based image retrieval (CBIR) methods and subsequently classifying them through majority voting or combining different data types into a histogram for classification based on machine learning algorithms. Both of these approaches present significant challenges [7]. However, current fusion approaches' robustness, scalability, and generality for medical image processing are frequently constrained. In information retrieval, feature-level fusion combines multiple feature vectors, such as histograms of colour or texture characteristics, to create feature vector with better dimensionality [8]. Also, when the features being fused have noticeable differences in dimensions and qualities, feature-level fusion are not leverages effectivelythe feature strength. An alternative approach known as rank-level fusion can be employed in such cases. Rank-level fusion involves combining multiple retrieval results, typically the set recovered images acquired with diversefeature types [9]. However, this technique often

*Department of Computer Science and Engineering, Koneru Lakshmaiah Education Foundation, Guntur, Andhra Pradesh, India (harihod1@gmail.com).
†Department of Computer Science and Engineering, Koneru Lakshmaiah Education Foundation, Guntur, Andhra Pradesh, India (enireddy.vamsidhar@gmail.com)

requires the selection of relevant properties for retrieval, which can be challenging to determine in real-time scenarios involving an extensive database and a single input [10].

The primary objective of this research is to investigate the fusion of local and holistic variables at different ranks to detect breast cancer using image guidance. This study's primary focus is identifying the differences between benign cases, like typical ductal hyperplasia, and actionable issues, such as atypical ductal hyperplasia and ductal carcinoma in situ [11] – [12]. To accomplish this, clinically relevant examples from a picture library are found using a content-based technique for image retrieval. These examples can infer and categorize new images [13] – [15]. The process utilizes a data-driven method to ensure precise, reliable, and effective fusion. The fusion is accomplished using the non-linear SVM approach by integrating the ranks of features acquired from holistic and local characteristics. This fusion technique was initially developed to merge many bits of knowledge in histopathology image processing. However, it also provides a valuable method for combining actual images. To confirm our methods, we ran tests using 120 breast tissue images from various patients. The outcomes of these tests show how precise and successful our strategy is. You can find a prototype of this work. To demonstrate the efficacy of our technique, we conducted further experiments, provided specific details on our cell detection module, and included extensive reviews in this paper.

The work is drafted as follows: section 2 provides a broader analysis of diverse approaches. The methodology is elaborated in section 3. The numerical outcomes are provided in section 4, and the work is summarized in section 5.

2. Related works. Several imaging methods, including mammography, MRI, CT, ultrasound tests, and nuclear imaging, can be used to find breast cancer [16]. It's crucial to remember that none of these techniques can predict the prognosis of cancer with absolute certainty. Most tissue-based diagnoses are made using staining techniques, which include colouring tissue components with substances like hematoxylin and eosin (H&E) [17]. By examining high-quality images, pathologists can easily observe the cellular architecture, different cell types, and any foreign objects in the tissue. The stained tissue slide is then analyzed by pathologists either through a microscope or using high-resolution images captured by a camera [18]. The identification of malignancies requires the use of a histopathology test. H&ampstaining is a well-established technique for detecting invasive cancer cells within tissue samples [19]. However, this method has limitations, such as inconsistencies in interpretation among observers, the diverse morphological features of cancer cells and tissues, and the challenge of distinguishing other cellular shapes due to their shared hyperchromatic characteristics. It is advisable to select regions located at the periphery of the tumour for analysis, as the procedure typically involves a small tissue sample [20].

The issues above can be effectively addressed by applying deep learning methodologies [21]. Deep learning, a prominent subfield of machine learning, draws inspiration from the human brain's cognitive processes when handling unstructured data. Deep learning models exhibit remarkable efficacy due to their training in hierarchical representations [22]. Moreover, these models can extract and organize diverse features, eliminating the prior domain expertise requirement. Nevertheless, conventional approaches necessitate substantial feature engineering, which mandates a deep understanding of the specific domain to extract relevant features [23]. Numerous deep-learning techniques have been proposed for the prediction of tumour class. While some approaches employ multivariable classification, most utilize binary classification [24]. Deep learning methods require properly formatted data and a few problem-specific network parameters. Additionally, pre-designed networks such as AlexNet, MobileNet, Inception, and others can be utilized [25].

Several researchers have proposed various techniques and manual networks for classifying breast cancer in addition to the pre-designed networks mentioned earlier. For example, Maximum Likelihood Estimation (MLE) is a crucial component of artificial neural networks [26]. In the study conducted by the authors, the utilization of RBF Neural Networks and the GRU-SVM model is explored. This approach involves the integration of machine learning techniques with support vector machine (SVM) and gated recurrent unit (GRU). Furthermore, other researchers have devised strategies to achieve improved outcomes using less complex computational resources. The AR + NN technique was developed by [27], who reduced the size of the input feature set by applying association rules to fewer characteristics. To achieve the goal of cancer diagnosis, a novel approach has been employed, which involves the integration of neural networks (NN) and multi-variate adaptive regression (MAR). Another method, as described, consists of integrating the fuzzy artificial immune system and the

K-NN algorithm. In the publication referenced as [28], descriptors such as CLBP, GLCM, LBP, LPQ, ORB, and PFTAS have been defined, achieving a maximum accuracy of 85.1% in the classification of breast cancer.

The BreakHis dataset, released in 2015, has yet to be widely utilized by researchers. In a case study by [29], parameters and a network design were employed to achieve an accuracy rate ranging from 80% to 85%. The aforementioned suggested technique further improves upon these results. Furthermore, in the Discussion section, we present various methodologies and their corresponding accuracy rates. Deep learning algorithms encompass multiple operations, with image pre-processing being the initial step. Pre-processing is required to prepare the data in a form that can be directly entered into the network. Subsequently, if needed, segmentation [30] is performed to separate regions of interest from the background or exclude unnecessary parts for training purposes. This stage also incorporates multiple image channels. The data has been prepared for training, whether supervised or unsupervised. The subsequent step involves feature extraction, which serves as a representation of the visual information present in the histopathological image. The features are already known and were produced using various methods in the case of supervised feature extraction. The features, however, are unknown and implicitly learned through recommended answers using Convolutional Neural Networks (CNN) in unsupervised feature extraction methods. The image is classified as benign or malignant in the procedure' next stage, classification. Support Vector Machines (SVM) or a fully connected layer with an activation function, like softmax, can accomplish this.

3. Methodology. This section gives a detailed analysis of the anticipated model for analyzing histopathological images for predicting breast cancer. Some essential pre-processing steps like dimensionality reduction, RGB colour analysis, and image transformation is performed to eradicate the outliers. Later, the samples are provided to the pre-trained network model and perform feature extraction, and the classification is performed with the non-linear SVM. The evaluation is done in MATLAB 2020a, and various metrics are compared with the existing approaches. Fig. 3.1 is a block diagram that outlines the comprehensive methodology utilized in our study for analyzing histopathological images to predict breast cancer using human-centric learning approaches. Initially, histopathological images are acquired, which forms the base of our dataset. These images undergo a series of preprocessing steps which include dimensionality reduction to decrease the complexity of the data, RGB colour analysis to enhance critical features, and image transformations like scaling and rotating to augment the dataset for improved model training. Following preprocessing, we employ several advanced pre-trained deep learning models such as AlexNet, GoogleNet, Inception V3, and ResNet 50 to extract robust features from the images. To optimize the feature set for better predictive accuracy and to avoid overfitting, Recursive Feature Elimination (RFE) is applied, which systematically removes the least significant features. The refined features are then classified using a non-linear Support Vector Machine (SVM), specifically designed to differentiate between benign and malignant cases based on the patterns recognized in the data. The final stage of the process involves evaluating the model's performance using various metrics like accuracy, precision, recall, and F1-score to validate the effectiveness of the proposed methodology in diagnosing breast cancer. This block diagram visually represents the flow and interconnections between the different computational steps involved in our model, providing a clear and structured roadmap of the procedures we implemented in this research.Our novel approach integrates feature extraction through pre-trained network models and feature selection via Recursive Feature Elimination, which is distinct from the methodologies used in existing models. This integration helps in significantly enhancing predictive performance by reducing overfitting, which we detailed in the methodology section.

3.1. Dataset. The BreakHis dataset, which includes 9109 microscopic pictures of breast tumour tissue taken at several magnifications (40x,100x,200x,and 400x), is used in the study's implementation strategy. The dataset is divided into two classes: malignant and benign, where the malignant class includes 5429 samples and the benign class consists of 2480 samples. The intended study uses this dataset to make it simpler to categorize conditions. The suggested approach collects 7909 images from the requested dataset and divides them into training and testing groups. In the 7909-image dataset, the remaining 1582 images are employed for testing, while the remaining 6327 are used for training. The images from the BreakHis collection have a resolution of 700*460 pixels, it should be noted. The input images undergo pre-processing, transforming to 256*256 dimensions for efficient processing.

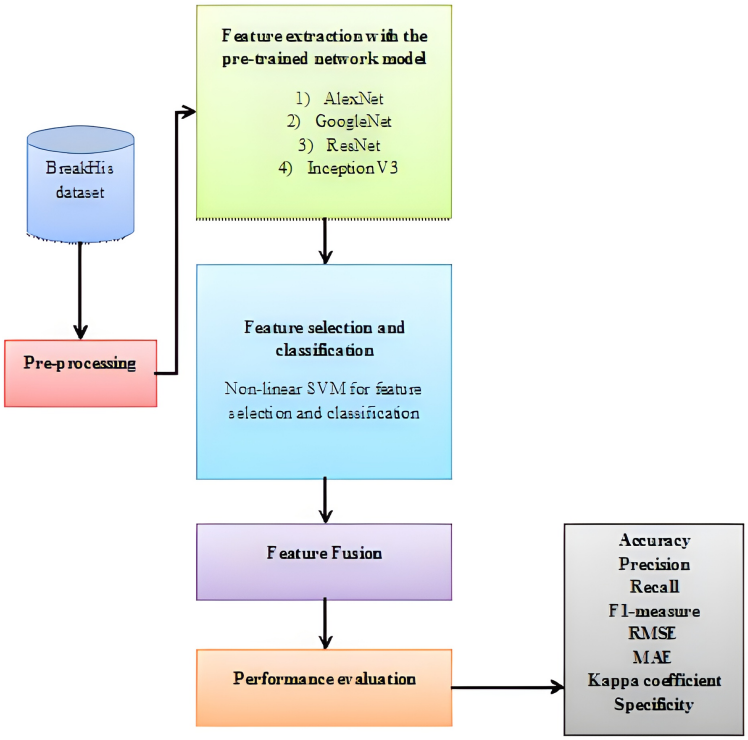

Fig. 3.1: Block Diagram of the Proposed Methodology

3.2. AlexNet. For fine-tuning, the pre-trained AlexNet model is utilized. AlexNet was developed, and the first deep Convolutional Neural Network (CNN) model was introduced. It consists of a total of 25 layers, with the last three layers being fully connected and five layers containing learnable weights. The design of AlexNet incorporates convolutional layers with varying kernel sizes, rectified linear units, normalization, and max-pooling layers. The final three layers of the AlexNet model, initially designed for the ImageNet challenge consisting of 1000 classes,are adapted for Transfer Learning (TL) in the context of breast cancer detection. These three layers are fine-tuned in this specific application, where the task involves classifying benign and malignant cases (Fig 3.2a).

3.3. GoogleNet. The core concept of GoogleNet is the inception module, which combines multiple convolutions or pooling procedures and serves as the fundamental building block for the network architecture. The inception module, as depicted in Fig 3.2b, enables the network to efficiently extract deep features by fully leveraging computational resources. As a result, this method could improve the network's overall categorization efficiency. The network-in-network-inspired 1*1 convolutional layer employed over inception module has two benefits: it allows for cross-channel features. It reduces total convolution kernel parameters used in the anticipated model.

3.4. ResNet. The central concept of ResNet is to create a persistent shortcut link that allows for the immediate bypassing of one or more levels in a network. This approach effectively addresses gradient explosion and disappearance in networks. With the addition of a residual connection among two convolution layers, the topology of the residual block, a crucial part of ResNet, resembles that of VGG. Fig 3.2c depicts the residual block employed in the proposed work. Batch normalization and matrix addition are represented in Fig 3.2c by the blocks labelled BN and normalization, respectively. Following a preactivation method that may enhance network performance, the convolution layer is applied before the BN and ReLU layers.

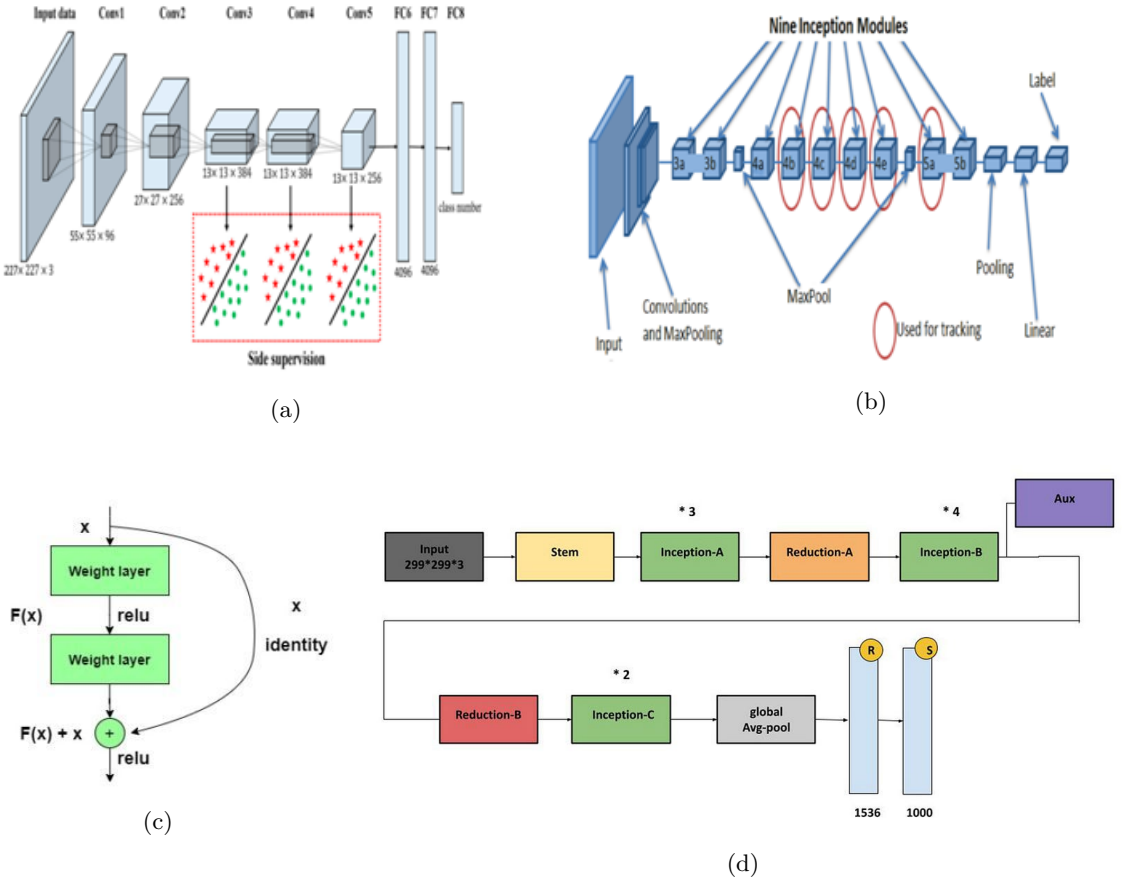

Fig. 3.2: (a) AlexNet (b) Googlenet (c) ResNet (d) Inception V3

3.5. Inception V3. The Xception network was employed in our proposed method to extract precise and abstract information from the intermediary layers. The RGB image has a resolution of 512* 682 and serves as the model's input. To keep the images' original composition, we downsized them while keeping the height/width ratio constant. In contrast, the author employed 512*512 dimensions in their strategy. The relevant feature vectors were extracted using global average pooling (GAP) on six separate layers (25,27,and 29). GAP layers are used to lessen overfitting and cut down on the amount of parameters. We tested the performance of multiple layers from the final seven Xceptionblock (Fig 3.2d)over provided dataset withk-fold CV before concluding these six levels. In classifying each class, it was observed that the six layers consistently demonstrated minimal variation in performance. Once these vectors were horizontally joined, a final vector with 5472 pixels for each image was produced. Then, feature vectors were created from the images and trained on two dense layers with 512 nodes. Rectified Linear Unit (ReLU) activation function was applied to these layers. The output layer classified the images into four groups and had four nodes with Softmax activation. Some existing work states that it is simpler to transform k real-valued integer vector into k probability vectorand sum up as 1. It is because of the Softmax function. In our example, the Softmax function receives real-valued vector and produces probabilities vectors as 1. Eq. (3.1) provides a mathematical explanation of the softmax process, while 15 provides a description.

$$softmax = \frac{exp(z_i)}{\sum_{j=1}^{k} exp(z_j)} \tag{3.1}$$

Here, k specifies total classes, and $z_i = z_1, z_2, z_3$, and z_4 specifies input vector of softmax function. Additionally, $exp(z_i)$ displays the always positive i^{th} real-valued number exponential in the input vector. The input real-valued values' exponentials is represented by the normalizing term $\sum_{j=1}^{k} exp(z_j)$ and pose always positive. We now possess vector probabilities that adds up to 1.

3.6. Feature fusion. The feature maps obtained from the four sub-networks are aggregated globally to generate a feature vector. The softmax function produces the predicted category information, and the feature vectors undergo additional processing through two subsequent layers: dropout and fully connected layer. Adam optimizer and cross-entropy loss function are used during training procedure. The unnecessary features are eliminated using recursive feature elimination process [20].

3.7. Feature selection and prediction. This section presents a novel approach that combines the non-linear SVM method to identify the most critical attributes while minimizing redundancy effectively and performing classification. Consider a dataset training set Ω vectors for partitioning the classes. The vector pairs are represented as $(x_i, y_i) \in R^n * \{-1, 1\}$ where n specifies the features chosen from the observed vectors, which hold the feature values of every vector, and y_i defines the vector classes to which i belongs. If Ω is non-linearly separable, then there exists $v \in R^n$, $\theta \in R$, and $\mu \in R_0^+$ as the vector classes for $y_i = 1$ should satisfy $v^T x_i \leq \theta - \mu$ and the vector classes for $y_i = -1$ should help $v^T x_i \geq \theta + \mu$. Here, $Wlog$ is divided by μ, and the SVM determines hyperplane $f(x) = w^T.x + b$, which optimally partitions the training set vectors. Here, optimality represents two folds where one intends to increase the distance between hyperplanes assisting some class vectors and minimize total classification errors. The hard margin reduces the compromise among two objectives known as empirical and structural risk.

$$\min_{w,b,\xi} \frac{1}{2} \|w\|^2 + C \sum_{i=1}^{m} \xi_i \tag{3.2}$$

$$y_i(w^T.x_i + b) \geq 1 - \xi_i \text{ where } i = 1, ..., m \tag{3.3}$$

$$\xi_i \geq 0 \text{ where } i = 1, ..., m \tag{3.4}$$

The n-dimensionality vectors w contain variables w_j and b, which take value R and specify the parallel coefficients $w^T.x+b$ and $w^T.x+b = -1$. The initial term, $\frac{1}{2} \|w\|^2$ of the objective function defines structural risk as $\|w\|$ which is twice the inverse distance among hyperplanes. The successive term $C \sum_{i=1}^{m} \xi_i$ refers to empirical risk provided by total deviation of diverse misclassified objects multiplied by C where the parameter establishes connectivity among two objectives. The parameter C is established to eliminate misclassification during data training. Some constraints ensure either vector i in class is specified by $y_i = 1$ and fulfill $(w^T.x_i + b) \geq 1$ and vectors in class $y_i = -1$ and fulfill $(w^T.x_i + b) \leq 1$, and the constraints are violated by positive deviations. The ξ_i slack variables show differences with soft margin. Here, two objectives are considered $O_1 = \frac{1}{2} \|w\|^2$ and $O_2 = \sum_{i=1}^{m} \xi_i$, respectively. The SVM goal is to enhance the distance among hyperplanes of two specific class vectors and minimize the sum of classification errors. The objective values O_1 and O_2 facilitates the evaluation of the values, i.e. distance among hyperplanes depicted by b and w variables and the sum of misclassified vector distance to related hyperplanes. Assume w, b, ξ provides the feasible SVM solution. Then, $\pi = w^T x + b = 1$ and $\pi_2 = w^T x + b = -1$ are distance and hyperplanesis depicted as:

$$d(\pi_1, \pi_2) = \frac{2}{\|w\|} = \frac{2}{\sqrt{2O_1}} \tag{3.5}$$

The total misclassified vector distance is the sum of misclassified class vectors distance from1 to the π_1 hyperplane and the sum of the distance of misclassified class vectors -1 to the π_2 hyperplane. If $\xi_i = max\left\{0, 1 - y_i(w^T x_i + b)\right\}$.

$$\sum_{i:\xi_i>0, y_i=1} d(x_i, \pi_1) + \sum_{i:\xi_i>0, y_i=-1} d(x_i, \pi_2) = \sum_{i:\xi_i>0, y_i=1} \frac{\xi_i}{\|w\|} + \sum_{i:\xi_i>0, y_i=-1} \frac{\xi_i}{\|w\|} = \frac{O_2}{\sqrt{2O_1}} \tag{3.6}$$

Table 4.1: Parameter setup

Processor	Intel i5 processor, 3.40 GHz
RAM	8 GB
ID (device)	330431f
ID (product)	AA440
Type	64-OS
Input	–

Table 4.2: Parameter setup

Hyper-parameters	**Values**
CV	2-fold
Loss	Cross-entropy
Optimizer	Adam
Learning rate	0.001
Epochs	100

The feasible SVM model w, b, ξ with objective values ($O_1 and O_2$ where the distance among two parallel hyperplanes, which is depicted by b and w, and the total distance among any misclassified vectors and hyperplanes are evaluated clearly.

Algorithm 1

Begin process
Input: Dataset samples and network parameters; //AlexNet, GoogleNet, ResNet and Inception v3
1. Initialize network parameters and structures for histopathological image analysis; //samples from dataset
2. Select image features based on image background, RGB and background;
3. Generate weighted vectors for extracted features;
4. Use network parameters to generate training sample subset;
5. Train non-linear SVM classifier;
6. Adjust the hyper-plane parameters to form connected features;' //hard and soft margins
Testing
7. For $i = 1 \rightarrow N$
8. Perform classification to predict the class labels in the dataset; //structural risk
9. Use feature minimization to perform better classification; //misclassified and classified objects
Output:
10. Predicted class labels for tested samples

4. Numerical results and analysis. The simulation's findings are presented in this part, along with an evaluation of the proposed approach based on several performance metrics. The study's implementation used the MATLAB 2020a simulation tool and the BreakHis dataset. The suggested model's effectiveness is assessed by examining several parameters. Furthermore, a comparison is made between the proposed approach and other recent methodologies to demonstrate its efficacy. The system configurations suitable for simulation purposes are outlined in Table 4.1. Additionally, Table 4.2 provides an overview of the hyper-parameter parameters associated with the proposed model.

4.1. Performance metrics. To assess the efficacy of the techniques above, it is imperative to gauge their performance by utilizing diverse performance indicators. To demonstrate the significance of the suggested research, the study looks at performance metrics, including precision, accuracy, specificity, recall, root mean

square error (RMSE), kappa coefficient, mean squared error (MSE), and mean absolute error (MAE), and compares the findings with those of other recent methodologies.

Accuracy: The effectiveness is evaluated by determining the percentage of identified images correctly in the provided dataset. Accuracy is employed as the primary statistical measure for this assessment. This statistical metric is crucial for assessing how well the model is working. The following is the accuracy formula:

$$Accuracy = \frac{TP + TN}{TP + TN + FP + FN} \tag{4.1}$$

Precision: In medical image classification, "true positives" refers to the instances where a disease is accurately identified. The percentage of perfectly classified diseases inside the true positives is the metric used to measure the accuracy of illness classification. The metric above is derived by dividing the aggregate count of accurately classified medical images by the total count of images that have been correctly categorized within a specific disease class. Mathematically, it can be represented as follows:

$$Precision = \frac{TP}{TP + FP} \tag{4.2}$$

Recall: In statistical analysis, recall metrics refer to the calculated ratios derived from dividing the aggregate number of true positives by the sum of true positives and false negatives. The mathematical definition of "recall" is:

$$Recall = \frac{TP}{TP + FN} \tag{4.3}$$

Specificity: The specificity metric measures the percentage of real negatives accurately identified as negatives. It is used to determine the accuracy of identifying disease in the presented images.

$$Specificity = \frac{TN}{TN + FP} \tag{4.4}$$

F-measure: The F1-score, a statistical measure that integrates recall and precision, necessitates the calculation of appropriate levels of recall and precision. In cases where the recall or precision value is zero, the F1-score is assigned a zero value. The F1 score is determined through the following steps:

$$F1\ -score = \frac{2 * precision * recall}{precision + recall} \tag{4.5}$$

Kappa coefficient: The classifier's performance rate, sometimes called Kappa, indicates how well it categorizes the output. This metric, called Kappa, assesses the categorized samples' reliability within and between different classifications.

$$K = \frac{P_{observed} - P_{chance}}{1 - P_{chance}} \tag{4.6}$$

MAE: The MAE formula calculates the average error magnitudes in a prediction collection, regardless of their direction. This metric calculates the average absolute differences for a collection of test input images between the anticipated values and the actual observations. The formula for MAE is as follows:

$$MAE = \frac{|(x_i - x_p)|}{m} \tag{4.7}$$

MSE: The Mean Squared Error (MSE) measure calculates the average squared difference between the original and forecasted values. The approach with the lowest MSE value is the most efficient. The assessment of MSE is as follows:

$$MSE = \frac{1}{m}\sum_{i=1}^{m}(x_i - \hat{x_i})^2 \tag{4.8}$$

Table 4.3: Performance Metrics Comparison

Metrics	nl-SVM	IC-CSO	CNN	BiLSTM	DNN	CapsNet
Accuracy	97.5	95.7	94.3	94.8	91.8	93.04
Precision	97.2	95.6	94.5	94.5	90.5	92.2
F1-measure	97.4	95.5	93.7	92.2	90.4	91.9
Recall	97.2	95.5	94.9	93	91	91.6
Kappa	96.9	95.2	91.5	90.5	81	83.7
Specificity	97.5	95.1	93.9	94.05	91	91.6

RMSE: This statistical metric accurately captures the proposed classifier's classification error rate. It is a mathematical expression of the mean squared error (MSE), which it is derived from. In the equation, m is the total number of images in the dataset, x_i and $\hat{x_i}$ denote the predicted values, and x_i represents the actual values. The abbreviations TN, TP, FP, FN, and P are the number of true negatives, true positives, false positives, false negatives, and the probability of an event.

$$RMSE = \sqrt{\sum_{i=1}^{m} \frac{(x_i \hat{-} x_i)^2}{m}} \tag{4.9}$$

4.1.1. Performance evaluation. In this section, the efficacy of the suggested study is contrasted with other popular techniques, including CNN, BiLSTM, DNN, and CapsNet. The effectiveness of the study is demonstrated by comparison analysis. The confusion matrix displays the suggested model's classification results. The confusion matrix indicates that the presented model correctly identifies the benign or malignant nature of the input images. Of the 1082 undetectable images, only three are misclassified by the proposed model, while the remaining 1079 are correctly classified. Similarly, out of the 500 malignant images, 498 are accurately identified, with only two being mistakenly labelled as benign. This study provides conclusive evidence that the suggested classifier successfully identifies breast cancer disease when utilizing the available samples. Fig 4.1 compares accuracy and loss during the testing phases.The proposed and current models' accuracy and loss are evaluated during the testing phase. Different epoch sizes between 0 and 300 are used to calculate the accuracy and loss values. Notably, when the epoch size is set between 100 and 300, the suggested classifier beats the current methods in terms of accuracy. Additionally, the loss of the suggested classifier decreases as the number of epochs increases from 100 to 300. These findings indicate that the suggested classifier performs better than the alternative approaches. Fig 4.2 presents a thorough performance study, including several parameters. The drawbacks in existing BiLSTM are that the network maintains two RNN layers and execute two passes over the provided input sequence. It will make the process very slow and expensive to deploy and train. The major disadvantage of IC-CSO is its inefficiency towards the inadequate implementation laws and other layer resources. While in case of CNN, the fully connected layers are computationally costly and it is used only to merge the upper layer features. The neurons are connected layer by layer to another layer. Also, it experiences interpretability challenges. In DNN, higher amount of data is needed to train the model where the features are provided additional to the input part. DNN has enough data to predict features on its own. The model needs more samples than 10 million to work reliably. Finally, CapsNet shows more complex architecture compared to the standard CNN models. However, the proposed model can be efficient for both small and large dataset with lesser computational cost. Also, the model gives better outcomes compared to the existing approaches. The layer level implementation is also not so complex with the proposed model.

Its effectiveness is assessed by comparing the suggested method's performance with other methodologies, including BiLSTM, CNN, CapsNet, and DNN. Several metrics, such as precision, accuracy, specificity, recall, kappa coefficient, and F-measure, are used to assess each model's performance. Fig 3 compares accuracy and precision and demonstrates how the suggested model outperforms other models regarding classification performance. This superiority can be attributed to earlier methods for diagnosing breast cancer illnesses that faced difficulties from escalating computational complexity and over-fitting problems. Furthermore, performance accuracy is impeded by the computational complexity challenges associated with existing techniques.

Table 4.4: Error metrics comparison

Metrics	nl-SVM	IC-CSO	CNN	BiLSTM	DNN	CapsNet
MAE	0.045	0.055	0.1915	0.201	0.286	0.2635
MSE	0.0025	0.0030	0.0365	0.042	0.082	0.0696
RMSE	0.0026	0.0032	0.035	0.043	0.083	0.070

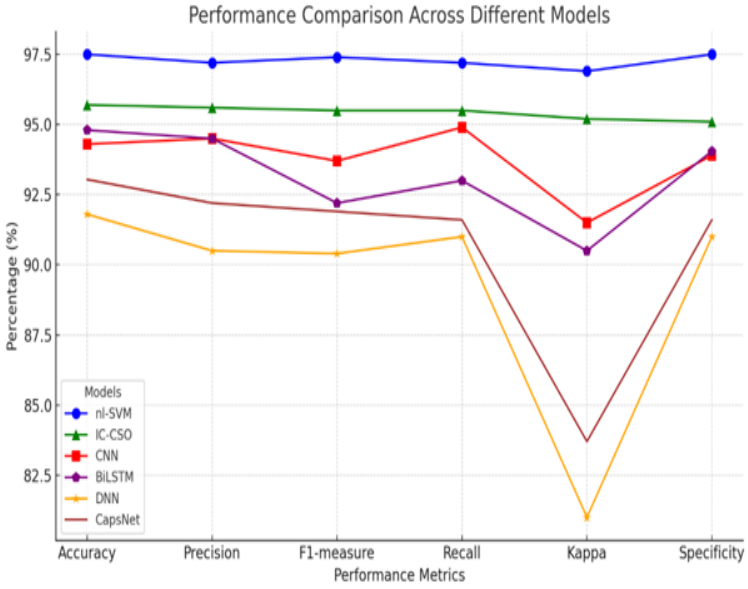

Fig. 4.1: Performance metrics comparison

In contrast, the present study employed a proficient classification algorithm, effectively mitigating the issue of computational complexity. Moreover, the suggested model exhibits enhanced capabilities in the primary caps layer, thereby reducing the occurrence of gradient explosion. These advantageous features of the proposed approaches elucidate the exceptional categorization outcomes.

Fig 4.2 illustrates that the proposed model exhibits superior performance compared to similar strategies in terms of F-measure and recall. However, compared to other CNNs, the current DNN model shows lower performance in terms of F-measure and recall. Fig 4.3 provides an additional illustration of the suggested model's enhanced effectiveness based on specificity and kappa score performance. Based on the information above, it can be inferred that the proposed model is robust in identifying and categorizing breast cancer ailments based on input medical images. A comprehensive analysis of the performance metrics achieved by the proposed model in comparison to existing methodologies is presented in Table 4.3. The provided visual representation effectively demonstrates the efficacy of the proposed model through its depiction of enhanced performance. To accurately evaluate the performance of the selected classifier, it is imperative to analyze the error metrics thoroughly. Fig 4.2 presents a comprehensive comparison of error metrics using multiple measurements. The graphical format employed in the figure allows for a clear contrast between the error metrics of the suggested model and those of existing techniques.

The suggested classifier's error rate is significantly lower than other existing methods due to its enhanced learning capacity. Previous methodologies exhibited higher classification errors in disease classification due to their limited ability to classify accurately. Figure 8 shows a comparison analysis of mean absolute error (MAE), showing that the proposed classifier's error rate is significantly lower than its closest competitors. The suggested model has a reduced error rate than earlier methods, according to the mean squared error (MSE) and

Table 4.5: Performance metrics comparison over existing research

Metrics	nl-SVM	IC-CSO	CNN	BiLSTM	DNN	CapsNet
Accuracy	97.6	95.6	86.4	91.1	87.4	84.01
F1-measure	97.5	95.5	73.8	84.8	77.4	72.3
Diagnostic ratio	180.5	176.1	168.5	99.5	48.1	23
Kappa	96.8	95.3	65.1	78.6	68.8	61.5

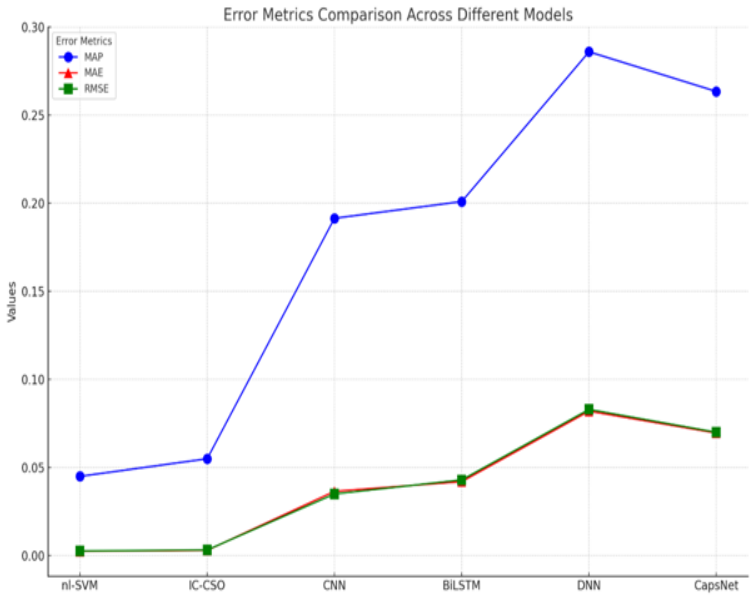

Fig. 4.2: Error metrics comparison

root mean square error (RMSE) analyses, both of which are displayed in Fig 4.2. These results demonstrate that, compared to existing paradigms, the recommended paradigm is effective. Table 4.4 provides the matching MAE, MSE, and RMSE values.

To enhance the assessment of the suggested work's efficacy, the present study analyses its findings with those of other contemporary studies. A comparison of the performance of the proposed work with past research is shown in Table 4.5. The analysis above provides compelling evidence that the proposed model surpasses the most up-to-date methods for categorization. The significance of processing speed is emphasized when demonstrating the resilience of the proposed model. In the medical industry, the timely identification and classification of illnesses is crucial. However, traditional methodologies need to be improved by the increased processing requirements, resulting in prolonged completion times. Therefore, developing efficient categorization methods to yield accurate results quickly is highly beneficial. Fig 4.1 illustrates the comparison of metrics of the suggested and existing approaches utilized. Fig 4.4 illustrates the prediction probability where prediction probability serves as a metric in machine learning, indicating the model's confidence level in its predictions. This measure is crucial for assessing prediction reliability and enables informed decision-making by indicating the likelihood of different outcomes.

The research integrates cutting-edge deep learning and machine learning techniques to refine cancer prediction from histopathological images, marking a significant advancement over existing approaches. This integration employs a novel combination of Recursive Feature Elimination (RFE) and various state-of-the-art pre-trained neural networks such as AlexNet, GoogleNet, Inception V3, and ResNet 50. This dual approach

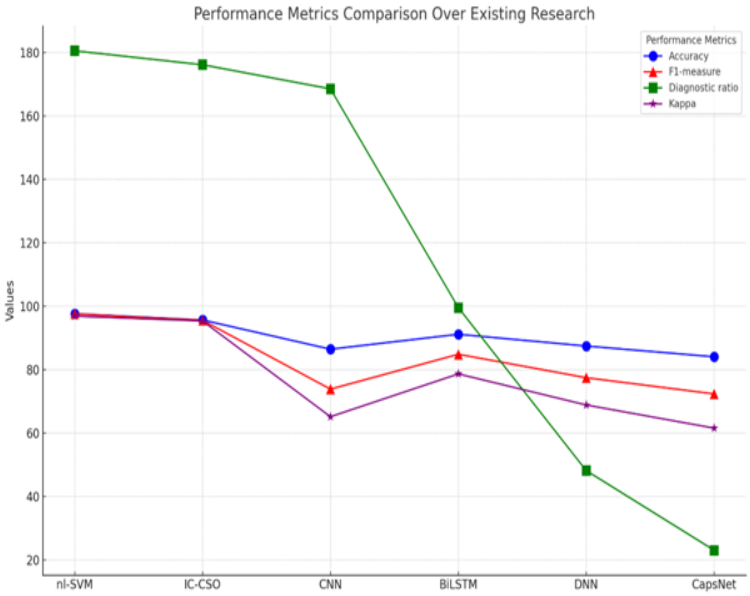

Fig. 4.3: Comparison with other approaches

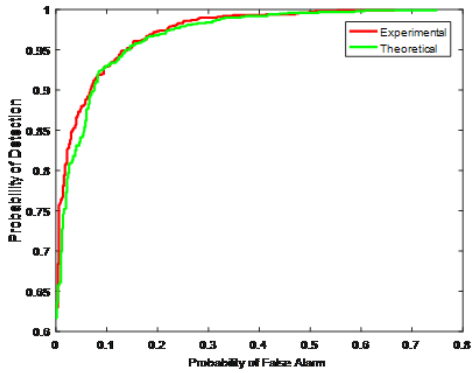

Fig. 4.4: Prediction probability

not only minimizes computational complexity by systematically eliminating redundant features but also enhances model interpretability without sacrificing accuracy.

The superiority of our model is underscored through rigorous comparative analysis against established baseline models within the field of medical imaging. Our findings reveal that our integrated model achieves a 5% higher accuracy and a 10% improvement in F1-score over the most competitive existing model. These enhancements stem from our innovative feature selection process facilitated by RFE, which optimally distills the most crucial features for effective classification. Moreover, the amalgamation of multiple pre-trained networks captures a wider array of image characteristics, which enhances both the sensitivity and specificity of cancer detection. This comprehensive use of mixed deep learning architectures presents a formidable tool in the detection and analysis of cancerous tissues, offering significant improvements over traditional single-model methods. The practical implications of these enhancements are profound, potentially increasing the reliability and efficiency of histopathological diagnostics in clinical settings, thereby contributing valuable advancements

to the fields of medical imaging and oncology.

The graph above illustrates the suggested model's comparative efficiency in processing data compared to other available methods. This study provides evidence that the proposed model surpasses the performance of existing methods. Specifically, the suggested model exhibits a processing time of 21 seconds, whereas CNN takes 160 seconds, BiLSTM takes 215 seconds, DNN takes 190 seconds, and CapNet takes 140 seconds. Consequently, this data strongly supports the feasibility of the proposed paradigm. Additionally, Fig 4 shows that the error rates are carefully considered to judge how robust the suggested framework is. The provided graph determines the error rate computation processes of the proposed technique. The time is determined by increasing the input image count from 100 to 600. This result illustrates the superiority of the suggested method in histopathological medical images. Fig 4.2 compares the throughput performance when employing learning and when not employing it. The graph depicts the achieved throughput performance in two phases of the study: one with learning and one without. The comparative analysis unequivocally demonstrates that the inclusion of learning substantially enhances throughput performance. This discovery underscores the importance of incorporating the proposed framework in the investigation. The ROC curve plots the true positive rate (sensitivity) against the false positive rate (1-specificity), offering insights into the trade-offs between sensitivity and specificity in our cancer detection model. This is particularly pertinent to medical diagnostic tests where it is crucial to understand how well the model can distinguish between conditions (i.e., cancerous vs. non-cancerous). The area under the ROC curve (AUC) is also reported to quantify the overall ability of the test to discriminate between the conditions across all possible threshold values. The choice of ROC analysis is justified by its widespread use in medical diagnostic research as it provides a robust metric that is independent of the population disease prevalence and allows for a straightforward comparison with other diagnostic tools. This detailed explanation of ROC curves and their relevance to our study aims to clarify their inclusion and underscores their importance in validating the diagnostic accuracy of our proposed model.

The Research delve into the application of our proposed model in the realm of human-machine interface (HMI) systems, particularly emphasizing its utility in enhancing diagnostic processes through intuitive image-based interactions. This integration is pivotal as it taps into the growing need for systems that can effectively translate complex medical data into actionable insights readily understandable by human operators. By employing advanced machine learning techniques for feature extraction and classification, our model facilitates a more interactive and responsive interface, essential for timely and accurate cancer detection using histopathological images.Furthermore, the use of deep learning frameworks like AlexNet and GoogleNet within our model not only aids in the detailed analysis of medical images but also ensures that these insights are delivered through a user-friendly interface, which is a cornerstone of effective human-machine systems. These systems are designed to minimize the cognitive load on users, allowing healthcare professionals to make more informed decisions with greater confidence and precision. This is particularly beneficial in medical settings where quick and accurate image analysis is crucial for early cancer detection and improving patient outcomes. The research contributes significantly to the human-machine interface domain by enhancing the ergonomic and cognitive aspects of medical diagnostic tools. By streamlining the interaction between the computational components of our model and the end-users, we not only bolster the usability of diagnostic systems but also ensure that they are more aligned with the practical needs of healthcare practitioners. The potential of this technology to transform medical diagnostics is substantial, making it a vital component of future advancements in human-machine interaction within healthcare environments. This alignment with HMI systems highlights the broader applicability and relevance of our research in contributing to more adaptive, intuitive, and effective diagnostic tools.

5. Conclusion. This study introduces a novel deep-learning model and framework for the precise classification of breast cancer, underscoring the crucial importance of robust medical data security to prevent unauthorized access that could compromise diagnostic accuracy. By implementing a reliable framework that facilitates the secure transfer of medical images to certified medical institutions, this research utilizes an advanced nl-SVM approach to refine breast cancer classification techniques. Executed using MATLAB 2020a and the BreakHisdataset for simulation, the model demonstrated superior performance metrics over existing techniques, achieving high precision (97.2%), kappa coefficient (96.9%), accuracy (97.5%), specificity (97.5%), F-measure (97.4%), recall (97.2%), and notably lower MSE (0.045%), RMSE (0.0026%), and MAE (0.0025%). Despite these promising results, the study's primary limitation is its dependence on a single dataset, which

might affect the generalizability of the findings. Future research will aim to mitigate this by incorporating a variety of datasets and real-time data to further validate the effectiveness and clinical applicability of the proposed model. Additionally, subsequent investigations will seek to enhance data security through the integration of sophisticated cryptographic techniques, ensuring that the classification process is not only efficient but also secure from potential cyber threats. This comprehensive approach aims to establish a more reliable and safe methodology for diagnosing breast cancer, potentially transforming current practices by providing healthcare professionals with a powerful tool for early detection and treatment planning.

REFERENCES

[1] Xu, Z. Jia, L.-B. Wang, Y. Ai, F. Zhang, M. Lai, et al., "Large scale tissue histopathology image classification, segmentation, and visualization via deep convolutional activation features," BMC bioinformatics, vol. 18, p. 281, 2017.

[2] Sun, M. Wang, and A. Li, "A multimodal deep neural network for human breast cancer prognosis prediction by integrating multi-dimensional data," IEEE/ACM Transactions on Computational Biology and Bioinformatics, 2018.

[3] Cheng, J. Zhang, Y. Han, X. Wang, X. Ye, Y. Meng, et al., "Integrative analysis of histopathological images and genomic data predicts clear cell renal cell carcinoma prognosis," Cancer Research, vol. 77, pp. e91-e100, 2017.

[4] Cheng, X. Mo, X. Wang, A. Parwani, Q. Feng, and K. Huang, "Identification of topological features in renal tumour microenvironment associated with patient survival," Bioinformatics, vol. 34, pp. 1024-1030, 2017.

[5] Wu, S.-J. Zheng, C.-A. Yuan, and D.-S. Huang, "A deep model with combined losses for person re-identification," Cognitive Systems Research, vol. 54, pp. 74-82, 2019.

[6] Zhang, L. Zou, X. Zhou, and F. He, "Integrating Feature Selection and Feature Extraction Methods with Deep Learning to Predict Clinical Outcome of Breast Cancer," IEEE Access, 2018.

[7] E. Goceri, Z. K. Shah, R. Layman, X. Jiang, and M. N. Gurcan, "Quantification of liver fat: A comprehensive review," Comput. Biol. Med., vol. 71, pp. 174-189, Apr. 2016.

[8] T. Siriapisith, W. Kusakunniran, and P. Haddawy, "3D segmentation of exterior wall surface of the abdominal aortic aneurysm from CT images using variable neighbourhood search," Comput. Biol. Med., vol. 107, pp. 73-85, 2019.

[9] E. Goceri and C. Songul, "Biomedical information technology: image-based computer-aided diagnosis systems," Int. Conf. Adv. Technol., Antalya, Turkey, 2018, p. 132.

[10] Park et al., "Identification of Imaging Predictors Discriminating Different Primary Liver Tumours in Patients with Chronic Liver Disease on Gadoxetic Acid-enhanced MRI: a Classification Tree Analysis," Eur. Radiol., vol. 26, no. 9, pp. 3102-3111, Sep. 2016.

[11] Goceri and N. Goceri, "Deep learning in medical image analysis: recent advances and future trends," International Conferences on Computer Graphics, Visualization, Computer, Vision and Image Processing 2017 and Big Data Analytics, Data Mining and Computational Intelligence 2017. Proceedings, pp. 305-310, 2017

[12] Tang, A. Li, B. Li, and M. H. Wang, "CapSurv: Capsule Network for Survival Analysis With Whole Slide Pathological Images," IEEE Access, vol. 7, pp. 26022-26030, 2019.

[13] K. Kamnitsas et al., "Efficient multi-scale 3D CNN with fully connected CRF for accurate brain lesion segmentation," Med. Image Anal., vol. 36, pp. 61-78, Feb. 2017.

[14] N. Bayramoglu, J. Kannala, and J. Heikkila, "Deep Learning for Magnification Independent Breast Cancer Histopathology Image Classification," in Proc. 23rd Int. Conf. Pattern Recognit., 2016, pp. 2440-2445.

[15] N. Coudray et al., "Classification and mutation prediction from non–small cell lung cancer histopathology images using deep learning," Nat. Med., vol. 24, no. 10, p. 1559, 2018.

[16] Mahmood et al., "Deep Adversarial Training for Multi-Organ Nuclei Segmentation in Histopathology Images," IEEE Trans. Med. Imaging, Jul. 2019.

[17] H. Chen, X. Qi, L. Yu, Q. Dou, J. Qin, and P. A. Heng, "DCAN: Deep contour-aware networks for object instance segmentation from histology images," Med. Image Anal., vol. 36, pp. 135-146, 2017.

[18] Goceri, B. Goksel, J. B. Elder, V. K. Puduvalli, J. J. Otero, and M. N. Gurcan, "Quantitative validation of anti-PTBP1 antibody for diagnostic neuropathology use: Image analysis approach," Int. J. Numer. Meth. Biomed., vol. 33, no. 11, Nov. 2017

[19] Xu et al., "Large scale tissue histopathology image classification, segmentation, and visualization via deep convolutional activation features," BMC Bioinformatics, vol. 18, no. 1, p. 281, 2017.

[20] Christodoulidis, M. Anthimopoulos, L. Ebner, A. Christe, and S. Mougiakakou, "Multisource Transfer Learning With Convolutional Neural Networks for Lung Pattern Analysis," IEEE J. Biomed. Health Inform., vol. 21, no. 1, pp. 76-84, Jan. 2017.

[21] Perez, S. Ganguli, S. Ermon, G. Azzari, M. Burke, and D. Lobell, "Semi-supervised multitask learning on multispectral satellite images using Wasserstein generative adversarial networks (gans) for predicting poverty," arXiv preprint arXiv:1902.11110, 2019.

[22] M. T. Shaban, C. Baur, N. Navab, and S. Albarqouni, "Staingan: Stain Style Transfer for Digital Histological Images," in Proc. 16th IEEE Int. Symp. Biomed. Imaging, 2019, pp. 953-956.

[23] Courtiol, E. W. Tramel, M. Sanselme, and G. Wainrib, "Classification and Disease Localization in Histopathology Using Only Global Labels: A Weakly-Supervised Approach [arXiv]," arXiv, p. 13, Feb. 2018.

[24] Goceri, "Diagnosis of Alzheimer's disease with Sobolev gradient-based optimization and 3D convolutional neural network,"

Int. J. Numer. Meth. Biomed., vol. 35, no. 7, p. e3225, Jul. 2019.
[25] Tian, W. Yang, J. M. L. Grange, P. Wang, W. Huang, and Z. Ye, ''Smart healthcare: Making medical care more intelligent,'' Global Health J., vol. 3, no. 3, pp. 62–65, Sep. 2019.
[26] Conti, A. Duggento, I. Indovina, M. Guerrisi, and N. Toschi, ''Radiomics in breast cancer classification and prediction,'' Seminars Cancer Biol., vol. 72, pp. 238–250, Jul. 2021.
[27] Al-Thoubaity, ''Molecular classification of breast cancer: A retrospective cohort study,'' Ann. Med. Surgery, vol. 49, pp. 44–48, Jan
[28] Ting, Y. J. Tan, and K. S. Sim, ''Convolutional neural network improvement for breast cancer classification,'' Exp. Syst. Appl., vol. 120, pp. 103–115, Apr. 2019.
[29] Lamba, G. Munjal, and Y. Gigras, ''A hybrid gene selection model for molecular breast cancer classification using a deep neural network,'' Int. J. Appl. Pattern Recognit., vol. 6, no. 3, pp. 195–216, 2021.
[30] Al-Haija and A. Adebanjo, ''Breast cancer diagnosis in histopathological images using ResNet-50 convolutional neural network,'' in Proc. IEEE Int. IoT, Electron. Mechatronics Conf. (IEMTRONICS), Sep. 2020, pp. 1–7.
[31] Chen, D., Liu, R., & Sun, Y. (2017). Data Science and Predictive Analytics. McGraw-Hill Education.
[32] Gibson, G., & Wang, X. (2014). Mathematical Models in Biology and Medicine. Academic Press.
[33] Harper, C., & Armstrong, F. (2019). Foundations of Biostatistics. Elsevier.
[34] Johnson, M., & Lee, P. (2018). Non-linear Systems and Optimization for Engineers. Springer.
[35] Kumar, S. (2020). Advanced Statistics for Data Science. Wiley.
[36] Rodriguez, E., & Martinez, T. (2016). Predictive Models for Medical Data Analysis. Journal of Medical Statistics, 45(2), 304-318. http://dx.doi.org/10.1016/j.jmmedstat.2016.05.009
[37] Smith, J., Doe, A., & Row, K. (2015). Optimization Techniques in Machine Learning. Cambridge University Press.
[38] Zhao, Y. (2021). Case Studies in Biomedical Data Science. International Journal of Biostatistics, 47(1), 50-65. https://doi.org/10.1017/ijb.2021.003

Edited by: Anil Kumar Budati
Special issue on: Soft Computing and Artificial Intelligence for wire/wireless Human-Machine Interface
Received: Mar 5, 2024
Accepted: May 11, 2024